JOURNAL OF SOLID STATE CHEMISTRY **121,** 117–128 (1996)
ARTICLE NO. 0017

Mechanism of Core Loss and the Grain-Boundary Structure of Niobium-Doped Manganese–Zinc Ferrite

Hideaki Inaba, Teruyoshi Abe, Yoko Kitano, and Junichi Shimomura

Technical Research Laboratories, Kawasaki Steel Corporation, Kawasaki-Chou, Chuo-ku, Chiba 260, Japan

Received May 2, 1995; in revised form August 18, 1995; accepted August 22, 1995

The mechanism of iron loss was investigated for Mn–Zn ferrites with and without Nb_2O_5 addition by observing the grain-boundary structure and measuring the various properties. Without Nb_2O_5 addition Ca and Si atoms concentrate near the grain boundary and are incorporated in the spinel lattice. With Nb_2O_5 addition Nb atoms concentrate in the grain boundary and keep Ca atoms from being incorporated in the spinel lattice. Hysteresis loss was reduced in spite of smaller magnetic permeability by the addition of Nb_2O_5. Eddy current loss and residual loss were reduced by the addition of Nb_2O_5, especially at high frequencies. The origin of the decrease in these losses was discussed on the basis of the data of the grain-boundary structure, permeability, electrical conductivity, and disaccomodation.

I. INTRODUCTION

Manganese–zinc ferrites have been widely used in electronic applications such as transformers, choke coils, noise filters, and recording heads, because of their high magnetic permeabilities and low magnetic losses. New power ferrites with low losses are needed for the transformers of switching power supplies in order to meet the demand for miniaturization of electric devices. Akashi (1) showed that the simultaneous addition of CaO and SiO_2 to Mn–Zn ferrites made electrical resistivity higher and improved magnetic properties. The additives of CaO and SiO_2 were reported to concentrate around the grain boundary to form a highly resistive layer. The thickness of the layer was reported to be 2 nm (2), 3–5 nm (3), and 1–5 nm (4) from the analysis of the concentrating Ca atoms. Otobe and Mochizuki (3) showed that the thickness of the layer was dependent on the quantity of the additives of CaO and SiO_2, sintering temperature, and heating rate of sintering. Tsunekawa *et al.* (4) showed that a large distortion of the spinel lattice near the grain boundary existed due to the incorporation of Ca atoms in the spinel lattice. It has been shown that the magnetic properties of Mn–Zn ferrites are greatly dependent on the small amount of additives such as CaO, SiO_2, V_2O_5, Nb_2O_5, Ta_2O_5 TiO_2, ZrO_2, and HfO_2, which affect the grain growth of the ferrites and the properties of the grain boundary (1–9). The addition of Ta_2O_5 in Mn–Zn ferrites was found to lower the power loss at high frequencies by many investigators (5–7). Znidarsic *et al.* (5) reported that Ta_2O_5 inhibited the grain growth and increased electrical resistivity by segregating at the grain boundary. Ishino *et al.* (6) reported that hysteresis loss as well as eddy current loss decreased by the addition of Ta_2O_5. They regarded the reason for this fact as due to the relatively higher density of the ferrite at the same grain size by the addition of Ta_2O_5. Otsuki *et al.* (7) investigated the additive effect of V_2O_5, Nb_2O_5, Ta_2O_5 TiO_2, ZrO_2, and HfO_2 and found that power loss at high frequencies decreased by forming a highly resistive layer at the grain boundary. They observed these additive atoms at the grain boundary, except for the case of TiO_2, by using transmission electron microscropy and energy dispersion X-ray analysis. Earlier, Franken and Doveren (9) had observed Ti atoms at the grain boundary by Auger electron spectrometry, probably indicating that some of Ti atoms may exist at the grain boundary. The addition of Nb_2O_5 in Mn–Zn ferrites is known to improve magnetic properties (7), but little is known of the mechanism of the additive effect of Nb_2O_5 on the magnetic properties.

In this study, magnetic properties of Mn–Zn ferrites with and without Nb_2O_5 addition were analyzed as a function of frequency. The mechanism on the magnetic effect due to the addition of Nb_2O_5 has been discussed on the basis of the analysis of the grain boundary using a transmission electron microscope and an energy dispersion X-ray analyzer.

II. EXPERIMENTAL PROCEDURE

Manganese–zinc ferrites in the formula $Zn_{0.26}Mn_{0.68}Fe_{2.06}O_4$ with and without Nb_2O_5 addition were prepared by the usual ceramic techniques. Sample A includes additives SiO_2, 180 ppm, and CaO, 350 ppm, and sample B includes Nb_2O_5, 280 ppm, in addition to these additives. The mixture of α-Fe_2O_3, Mn_3O_4, and ZnO in the molar ratio of 52.5, 35.5, and 12.0 was ground to mix with a ball-

0022-4596/96 $12.00

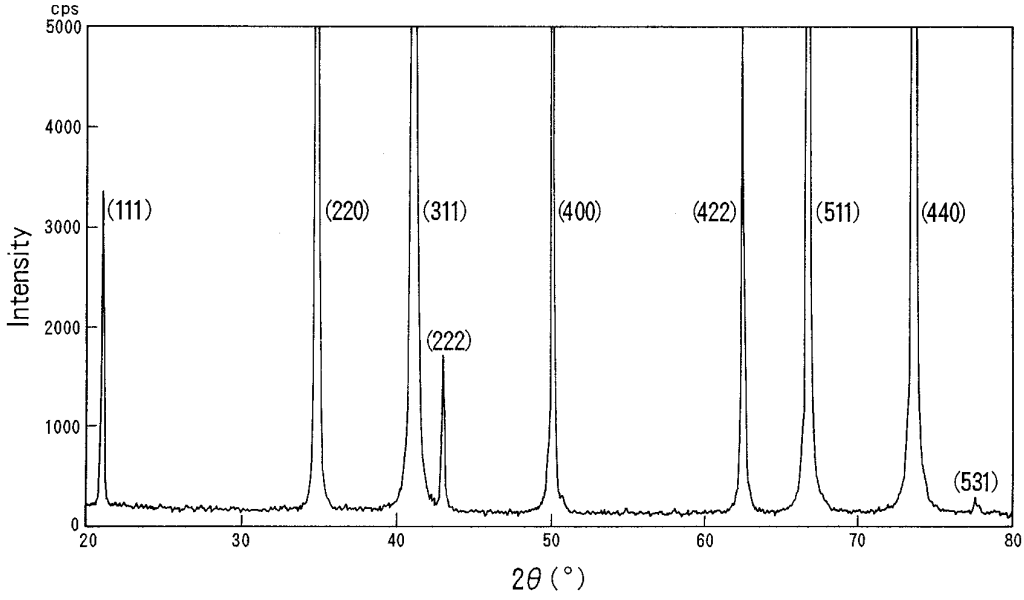

FIG. 1. X-ray diffraction pattern of an Mn–Zn ferrite (sample A). Sample B also shows essentially the same pattern.

mill using steel balls and prefired for 1 h at 1173 K. The α-Fe_2O_3 powder was provided by Kawasaki Steel Corporation (KH-UP) and included 40 ppm SiO_2. The prefired powder was ground to 1.2 μm with a ball-mill using steel balls and adding $CaCO_3$ (600 ppm), SiO_2 (100 ppm), and Nb_2O_5 (280 ppm or none) and was pressed at 1 ton cm^{-2} in toroids with 35 mm outer diameter, 25 mm inner diameter, and 8 mm height, with a density of 2.8 g cm^{-3}. The pressed samples were heated at a rate of 200 K h^{-1} under air to 1373 K and at a rate of 300 K h^{-1} under a partial oxygen pressure (P_{O2}) of 0.01 bar to 1593 K, kept 3 hr under P_{O2} of 0.05 bar and then cooled at a rate of 100 K h^{-1} under P_{O2} of 0.02 bar to 1473 K, under P_{O2} of 0.002 bar to 1373 K, and under nitrogen atmosphere to room temperature. The X-ray diffraction pattern for sample A, which is shown in Fig. 1, indicates a cubic spinel phase with a lattice constant of 0.8497 nm. The ratio between Fe^{2+} and the total Fe was determined to be 0.046 and 0.045 for samples A and B, respectively, by chemical analysis (10, 11). The contents of Zn and Mn were also determined by chemical analysis (12, 13). The error of each chemical analysis was estimated as 0.06%. Then the formula of the composition can be written as $Zn_{0.26}Mn_{0.68}Fe^{3+}_{1.965}Fe^{2+}_{0.095}O_4$. The larger content of total Fe compared with the initial mixture is considered to come from the steel balls during the mixing and grinding processes.

The observation of lattice image and the analysis of concentrations of various atoms near the grain boundary were conducted by using a field emission transmission electron microscope (FE-TEM). The samples for the FE-TEM were made by ion milling and the observation of lattice images, and the analysis of relative concentrations of various atoms near the grain boundary were conducted at the tilting angle of the smallest width of the grain boundary so that the electron beam would be parallel to the grain boundary surface with adjustment of a tilting stage. The compositional analysis of small areas of the samples was made by energy dispersion X-ray (EDX) analyzer and the intensities of EDX were converted theoretically to the relative concentrations. Various properties such as magnetic permeability and power loss as a function of frequency, hysteresis loss, disaccomodation, and electrical conductivity were measured on these samples.

III. RESULTS

The lattice image of sample B is shown in Fig. 2, where the image of cubic spinel lattice and a grain boundary are seen. The areas marked by circles and numbers from 2 through 10 shown in Fig. 2 were analyzed by energy dispersion X-ray (EDX) analyzer and the results are shown in Fig. 3, where Nb atoms along with Ca and Si atoms concentrate at and near the grain boundary with a half-width of 2.5 nm. Niobium and Ca atoms are not incorporated in the spinel lattice, although Si atoms are slightly present in the spinel lattice. An example of the precipitation of a crystalline phase around the grain boundary is shown in Fig. 4. The results of EDX analysis and the pattern of light diffraction on the middle part of the crystalline phase are shown in Figs. 4a and 4b, respectively. The lattice spacings 0.32 and 0.39 nm were close to 0.306 and 0.387 nm, respec-

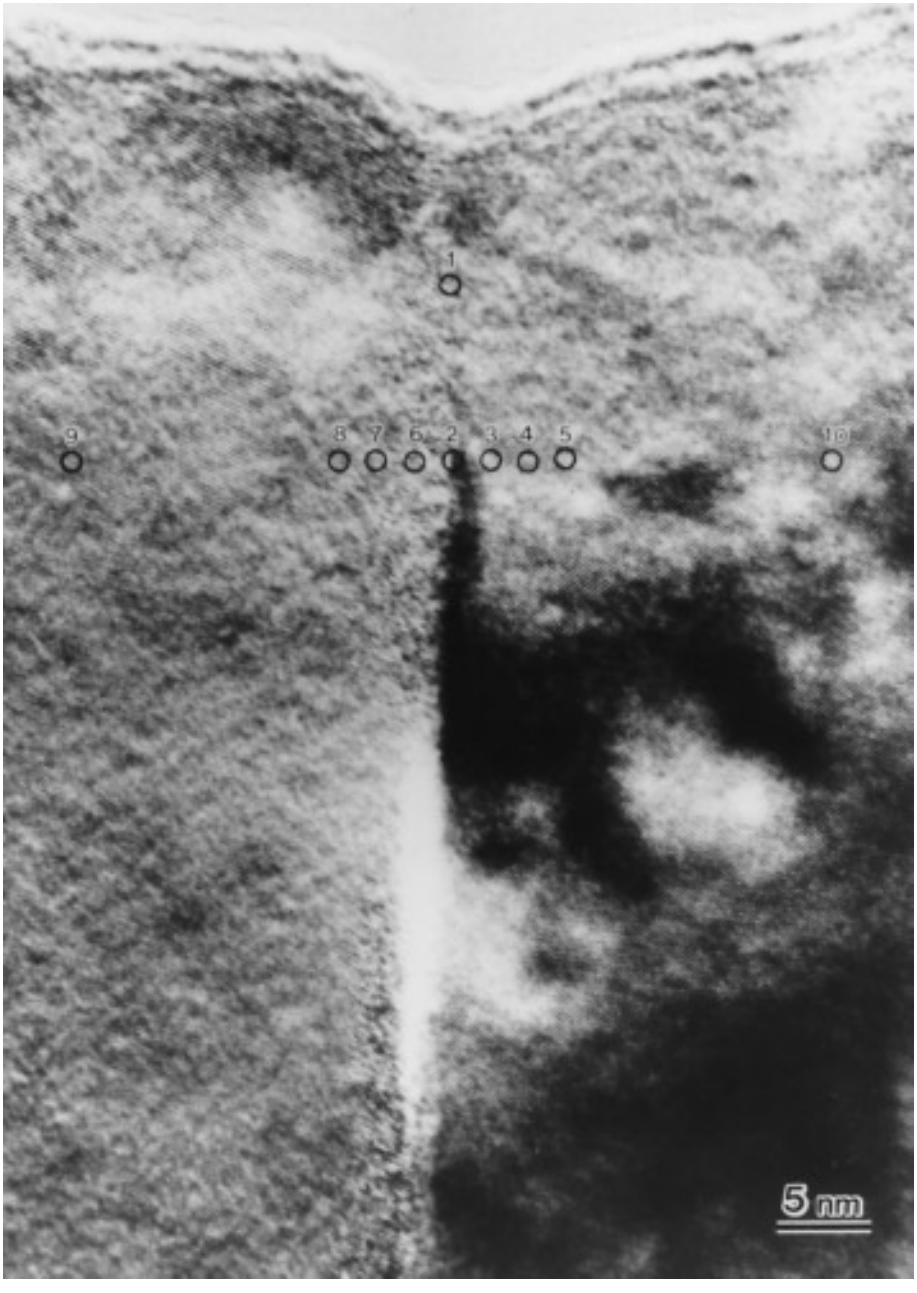

FIG. 2. Lattice image of an Mn–Zn ferrite with Nb_2O_5 addition (sample B). A grain boundary is seen in the center of the figure. Circles and numbers indicate the points of EDX analysis shown in Fig. 3.

tively, which are from (131) and (−101) reflection of orthorhombic $CaNb_2O_6$, and the crystalline phase around the grain boundary can be assigned as the $CaNb_2O_6$-type partially substituted by divalent Fe, Mn, and Zn atoms in place of Ca atoms. The chance for such a crystalline phase to appear around the grain boundary was very rare in the present sample, but it increased and the area of the crystalline phase increased when the addition of Nb_2O_5 was increased. The analysis of the triple junctions was also conducted and the EDX analysis was similar to Fig. 4a, but changed depending on the position. The precipitations at the triple junctions seems to be composed of the $CaNb_2O_6$-type and the related crystalline phases.

The lattice image of sample A (without Nb) is shown in Fig. 5, where the lattice image of the spinel lattice is clearly seen even in the area very close to the grain

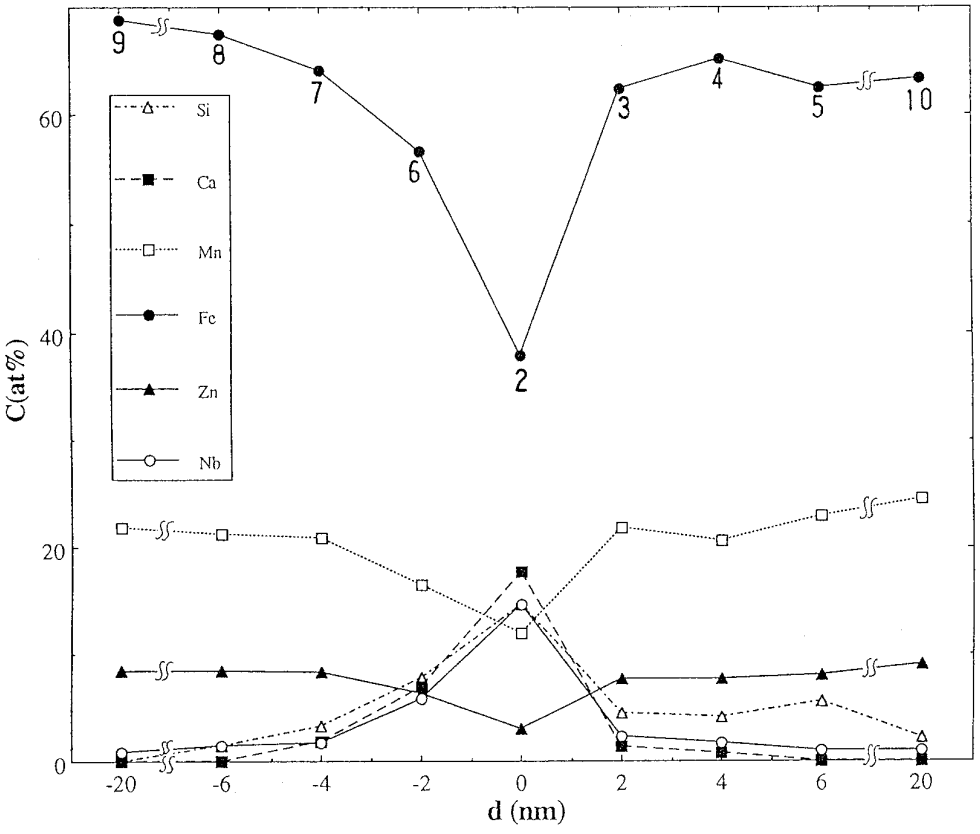

FIG. 3. EDX analysis near the grain boundary shown in Fig. 2. Relative atomic concentrations are shown as a function of the distance from the grain boundary. Numbers marked in the figure indicate the points shown in Fig. 2.

boundary. The EDX analysis was also conducted in the areas marked by circles and numbers from 1 to 11 shown in Fig. 5 and the results are shown in Fig. 6. In this case, Ca and Si atoms are incorporated in the spinel lattice as far as 6 nm (half-width). This result is considered to be compatible with the result of Tsunekawa *et al.* (4), where the lattice parameter increases near the grain boundary due to the incorporation of Ca atoms in the spinel lattice.

The results of electrical conductivity measurement are shown in Fig. 7 as a function of inverse temperature. The electrical conductivity of sample B is considerably smaller with a higher activation energy of 0.211 eV compared with sample A (0.176 eV).

The density of undoped and doped samples was determined by the Archimedes' method as 4.91 and 4.87 g cm^{-3}, respectively. The average grain size of undoped and doped samples was determined as and 9.0 and 9.2 μm, respectively from the photograph of a microscope using the samples chemically etched by hot HCl. The scanning electron microscopy pictures were taken for both samples, and no difference in microstructure elements such as grain and pore size distribution was found between them except for the small difference in the grain size. The addition of Nb_2O_5 is thought to slightly promote the grain growth.

Initial permeability was measured for the samples with and without Nb_2O_5 addition and the results are shown in Fig. 8 as a function of frequency. Initial permeability of sample B was about 15% smaller than that of sample A and the resonance frequency due to the resonance of domain wall motion and/or spin rotation became higher by the addition of Nb_2O_5.

Power losses (PL) at 200 mT for DC (hysteresis loss) and 100 kHz were measured and the results are shown in Fig. 9 as a function of temperature. Power loss of sample B at 100 k Hz was about 12% smaller than that of sample A. The hysteresis loss of sample B was also smaller by several percent than that of sample A, although the permeability for sample B was considerably small compared with sample A (see Fig. 8). The eddy current loss plus residual loss for sample B is also smaller than that of sample A, as shown in Fig. 9, since the power loss is the sum of contributions of hysteresis loss P_h, eddy current loss P_e, and residual loss P_r. The power loss was also measured as a function of frequency at 50 and 200 mT and 50°C, and

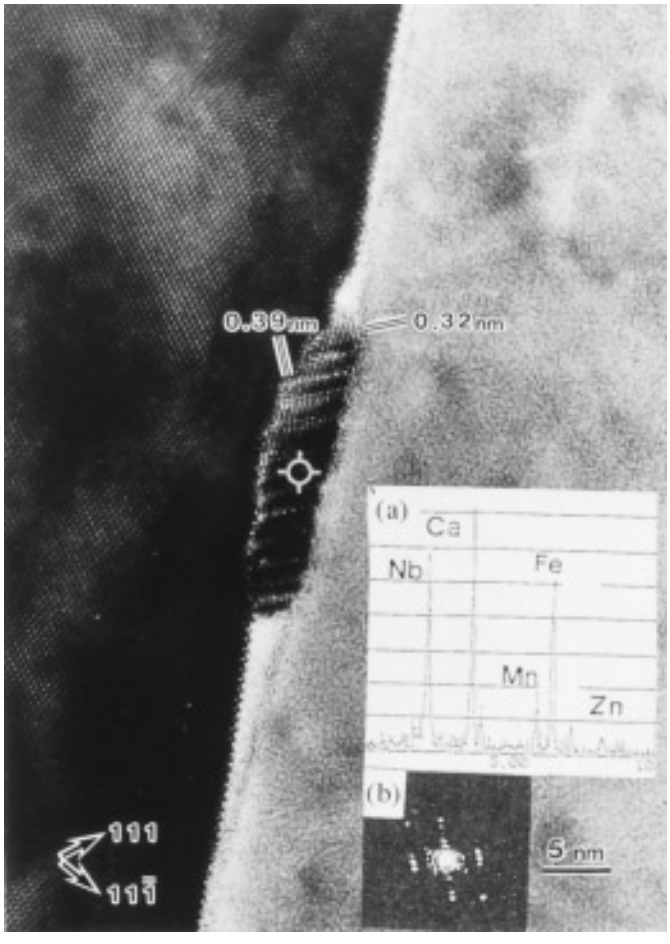

FIG. 4. An example of the precipitation of $CaNb_2O_6$-type phase around the grain boundary. (a) EDX analysis of the middle part of the crystalline phase marked by ⊕. (b) The pattern of light diffraction from the middle part of the crystalline phase marked by ⊕.

the results are shown in Figs. 10 and 11, respectively. The power loss divided by frequency is plotted in these figures as a function of frequency according to the equation

$$\mathrm{PL}/f = K_\mathrm{h} + K_\mathrm{e} \cdot f + K_\mathrm{r}(f), \qquad (1)$$

where K_h and K_e are the coefficients due to the hysteresis and eddy current loss, respectively, and K_r is the coefficient due to the residual loss, which is considered to be dependent on frequency f. As seen in Fig. 11, the power loss of sample B is about 10% smaller compared with sample A below 200 kHz, and becomes much smaller at higher frequencies. Using the data at and below 200 kHz at 200 mT, where the linear relationship holds for both samples in Fig. 11, K_h and K_e for samples A and B are determined by the least-square method as 1.42 and 1.33 kW m^{-3} (kHz)$^{-1}$ and 0.0167 and 0.0154 kW m^{-3} (kHz)$^{-2}$, respectively. The hysteresis losses thus calculated are in good agreement with the results of the direct measurement shown in Fig. 9, although the absolute values obtained by both methods are slightly different.

The temperature dependence of disaccommodation (DA) was measured for samples A and B in order to compare the magnitude of the magnetic aftereffect as a function of temperature. The DA is defined here as $\mathrm{DA} = (\mu_0 - \mu_{20})/\mu_0$, where μ_0 and μ_{20} are permeability at 10 sec and 20 min after demagnetization, respectively, at the frequency of 100 kHz. The results are shown in Fig. 12. Figure 12 shows that the addition of Nb_2O_5 reduces disaccommodation by about 30% in the temperature range of the measurement.

IV. DISCUSSION

1. Structure and Ionic Distribution around the Grain Boundary

As described in the previous section, in the case of the sample without Nb_2O_5 addition, Ca and Si atoms are incorporated in the spinel lattice as far as 6 nm (half-width) and the lattice parameter is thought to increase near the grain boundary due to the incorporation of Ca atoms in the spinel lattice, according to Tsunekawa *et al.* (4). In the case of the doped sample with Nb_2O_5, however, Nb atoms concentrate in the grain-boundary region and keep Ca and Si atoms from being incorporated in the spinel lattice. These phenomena would be explained by the pair of Nb^{5+} and Ca^{2+} ions around the grain boundary as expected from the existence of $CaNb_2O_6$-type phase around the grain boundary (see Figs. 3 and 4) in order to keep the charge balance, since the average charge of the cation sublattice of the spinel is 2.67. The pair of Nb^{5+} and Ca^{2+} ions around the grain boundary in such a way would decrease the distortion in the spinel lattice.

The enrichment in Nb around the grain boundary would also make the pairs of Nb^{5+}–Fe^{2+}, Nb^{5+}–Mn^{2+}, and Nb^{5+}–Zn^{2+} to form a compound like (Ca, Fe, Mn, Zn) Nb_2O_6 in order to keep the charge balance as expected from the existence of $CaNb_2O_6$-type phase partially substituted by divalent Fe, Mn, and Zn atoms in place of Ca atoms around the grain boundary (see Fig. 4). Among these pairs Nb^{5+}–Ca^{2+} is thought to be the most strongly bound, because the distribution of Ca atoms is most similar to that of Nb atoms around the grain boundary according to Figs. 3 and 4. It is also noted that among these pairs Nb^{5+}–Fe^{2+} (loosely bound) would have the most important effect on the magnetic properties, since the anisotropic constant of Mn–Zn ferrites is mainly determined by the content of Fe^{2+} ions and the electrical conductivity of Mn–Zn ferrites is mainly determined by the hopping of electrons between Fe^{2+} and Fe^{3+} ions. Since the concentration of Fe^{2+} ions

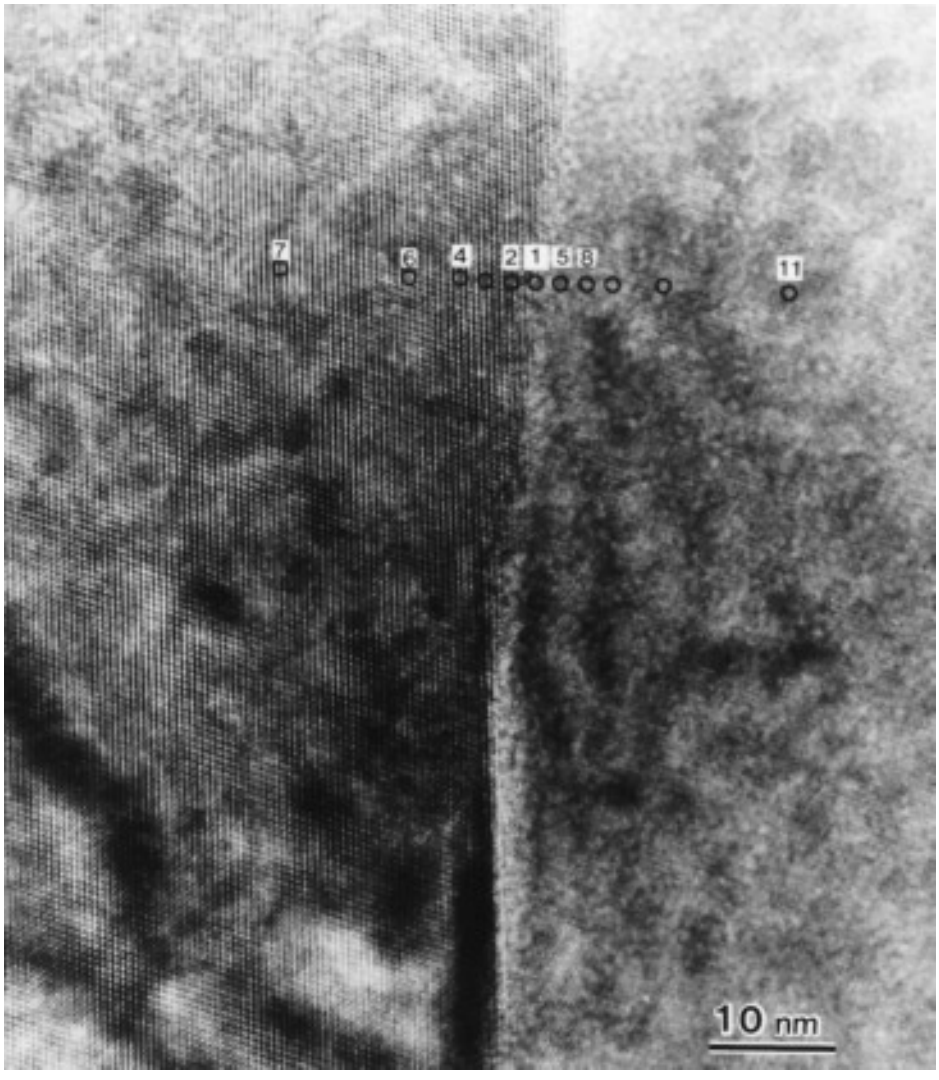

FIG. 5. Lattice image of a Mn–Zn ferrite without Nb_2O_5 addition (sample A). A grain boundary is seen in the center of the figure. Circles and numbers indicate the points of EDX analysis is shown in Fig. 6.

is nearly the same in both samples (A and B) according to the chemical analysis and Fe^{2+} ions are localized around the grain boundary in sample B, the concentration of Fe^{2+} ions in the bulk of sample B should be less than that of sample A. The smaller electrical conductivity and the higher activation energy for sample B as shown in Fig. 7 would be explained to be due to the localization of Fe^{2+} ions which are loosely bound by Nb^{5+} ions.

2. *Additive Effect of Nb_2O_5 on the Grain Growth of Mn–Zn Ferrites*

The addition of Nb_2O_5 slightly stimulates the grain growth of Mn–Zn ferrites. Kin and Im (14) reported that the addition of Nb_2O_5 stimulated the sintering of Li–Zn ferrites, although the reasons for this were not given. Recently, the melting points (15) for samples with (Fe, $Mn)_3O_4$–Nb_2O_5 and (Fe, Mn, $Zn)_3O_4$–(CaO, SiO_2)–Nb_2O_5 systems were measured using differential thermal analysis, and it was found that the melting points were decreased by about 200 K in the former and 50 K in the latter system. The lowering of the melting point would increase the volume of liquid in the grain-boundary region and stimulate liquid-phase sintering. The larger grain size by the addition of Nb_2O_5 should make the initial permeability greater, but the experimental results are the opposite, as shown in Fig. 8. The reason for this will be discussed next.

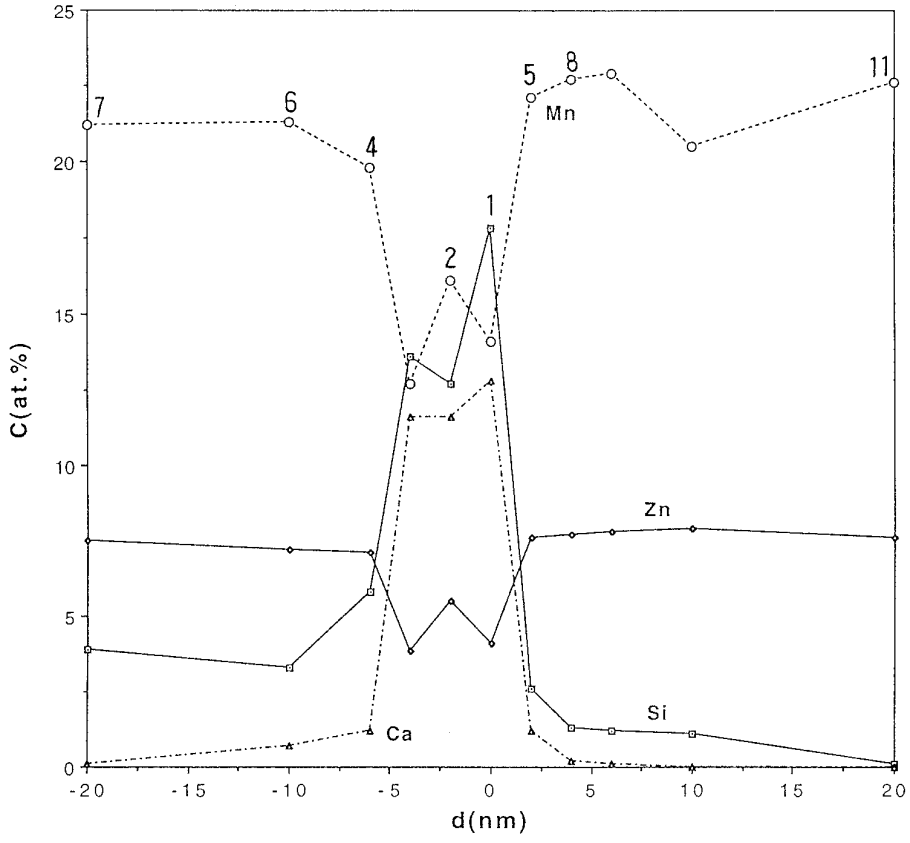

FIG. 6. EDX analysis near the grain boundary shown in Fig. 5 (sample A). Relative atomic concentrations are shown as a function of the distance from the grain boundary. Numbers marked in the figure indicate the points shown in Fig. 5.

3. Initial Permeability and Hysteresis Loss

As seen in Figs. 8 and 9, the addition of Nb_2O_5 makes initial permeability lower and hysteresis loss at 200 mT lower. This is rather contradictory, because high initial permeability is due to the easy wall motion and/or spin rotation and the easy wall motion and/or spin rotation should make hysteresis loss low in a general sense. There may be three factors due to the additive effect of Nb_2O_5 which influence initial permeability and hysteresis loss. One is the grain size, the second is Fe^{2+} content and distribution, and the third is the internal stress due to the lattice distortion. First, the larger grain size would make the initial permeability higher and hysteresis loss lower, but this effect may be small because the difference in grain size between A and B is rather small. Second, Nb_2O_5 addition makes the content of Fe^{2+} ions in the bulk lower, as a result of the loose pairing of Nb^{5+} and Fe^{2+} ions around the grain boundary, and may make the anisotropy constant larger as a result of the improper content of Fe^{2+} ions in the bulk, which would make permeability lower and hysteresis loss higher. Third, Nb_2O_5 addition makes the internal stress due to the lattice distortion smaller due to the pairing of Nb^{5+} and Ca^{2+} ions around the grain boundary, which would make permeability higher and hysteresis loss lower. The lower permeability of sample B may be ascribed to the predominant effect of the second factor and the lower hysteresis loss may be ascribed to the predominant effect of the third factor, although the reason for this is not clear at present.

4. Eddy Current Loss and Residual Loss

As seen in Figs. 10 and 11, the smaller power loss of sample B at high frequencies is mainly due to the smaller contribution of eddy current loss and residual loss compared with sample A. With the addition of Nb_2O_5 eddy current loss is considered to be smaller due to the higher resistivity, as seen in Fig. 7. The origin of the higher resistivity in sample B would come from the smaller chance of hopping between Fe^{2+} and Fe^{3+} ions, because Fe^{2+} ions are considered to be loosely bound with Nb^{5+} ions around the grain boundary.

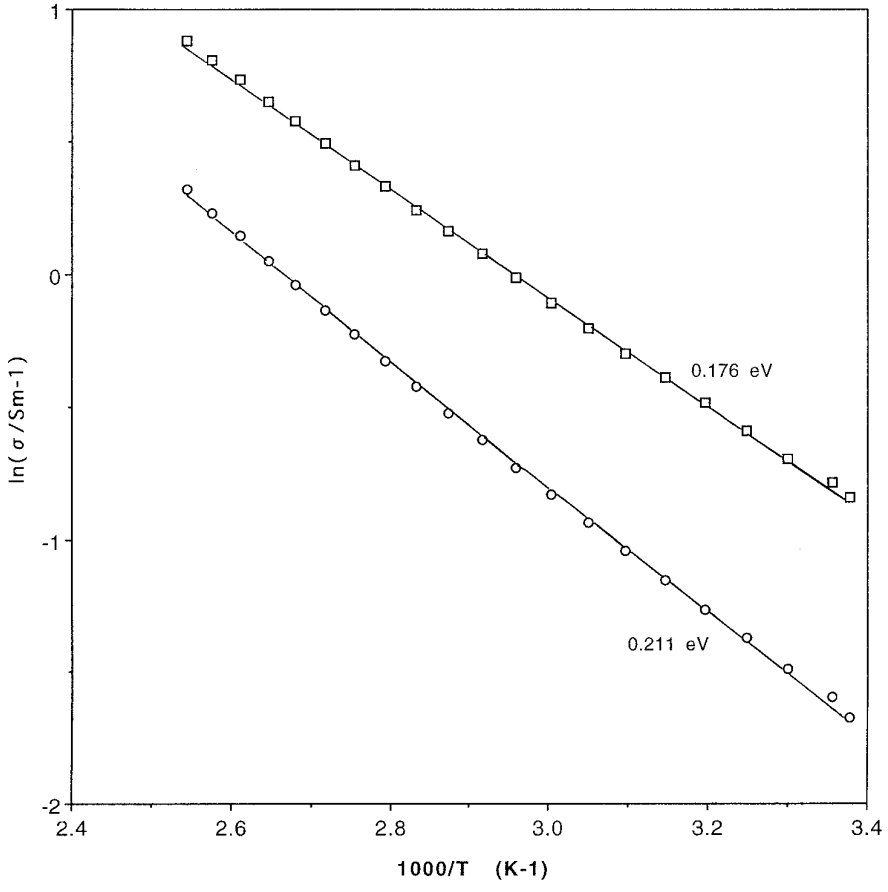

FIG. 7. Electrical conductivity as a function of inverse temperature. □, sample A; ○, sample B.

In the analysis shown in Equation [1], we estimate the eddy current loss from the slope of the line shown in Figs. 10 and 11 assuming that electrical resistivity is not dependent on frequency. However, AC resistivity of Mn–Zn ferrites is decreased considerably at high frequencies, as reported by Sato and Sakaki (16). In the present paper, we include this contribution in residual loss. When the frequency becomes higher than 500 kHz, the contribution due to residual loss becomes higher, as seen in Figs. 10 and 11. The origin of the residual loss has been considered to be (1) the capacitance component of AC resistivity mainly coming from the grain-boundary layer, (2) resonance and relaxation due to the domain wall motion and/or spin rotation, (3) the component due to the diffusion magnetic aftereffect, and (4) dimensional resonance, but the quantitative analysis of these contributions has not been accomplished yet. Sato and Sakaki (16) tried to show that the capacitance component was the main contribution of residual loss, and the theoretical explanation was made with qualitative success, but not quantitative success. Since the measurement of AC resistivity as a function of frequency has not been done in the present study, it is not possible to show how much this component contributes to the residual loss.

The addition of Nb_2O_5 is considered to reduce the contribution due to the resonance of domain wall and/or spin rotation, since initial permeability became smaller and the resonance frequency shifted to the higher side by the addition of Nb_2O_5, as shown in Fig. 8.

The migration of Fe^{2+} ions into cation vacancies at high magnetic flux and high frequencies is thought to become one component of magnetic loss. Such a component would be estimated from the measurement of disaccommodation, because the migration of Fe^{2+} ions into cation vacancies is thought to be the main mechanism of DA around room temperature (17). As seen in Fig. 12, the DA of sample B (Nb_2O_5 addition) is about 30% smaller than that of sample A. The migration of Fe^{2+} ions into cation vacancies is thought to be suppressed by the addition of Nb_2O_5, since Fe^{2+} ions are thought to be loosely bound with Nb^{5+} ions. The smaller magnetic aftereffect in the sample with the addition of Nb_2O_5 is considered to reduce the residual contribution of power loss at high frequencies.

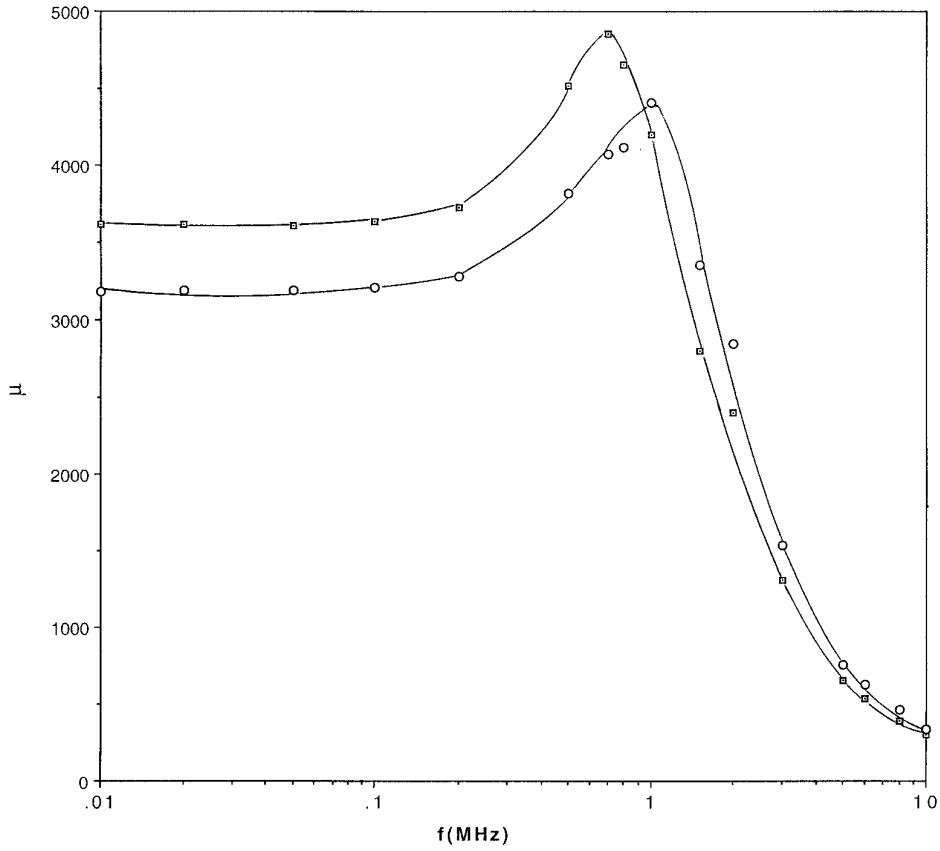

FIG. 8. Initial permeability as a function of frequency at room temperature. (□) sample A; (○) sample B.

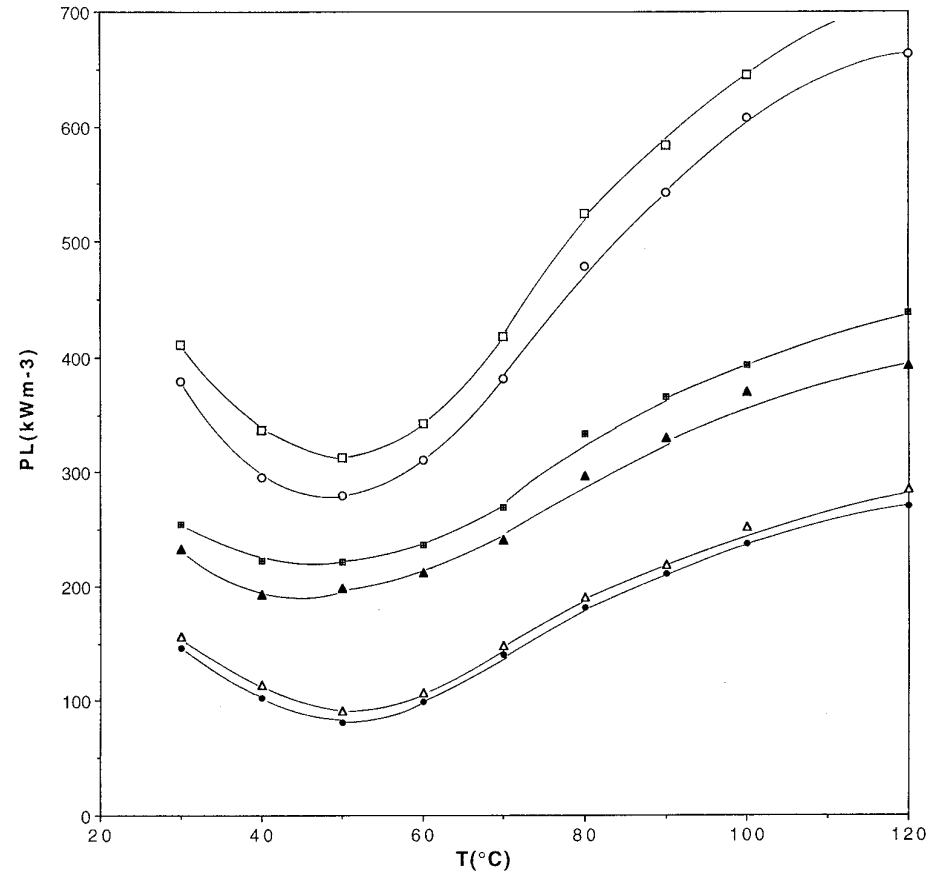

FIG. 9. Power losses at 200 mT for DC and 100 kHz as a function of temperature. (□, ○) PL at 100 kHz for samples A and B, respectively. (△, ●) P_h for samples A and B, respectively. (■, ▲) (P_e + P_r) for sample A and B, respectively.

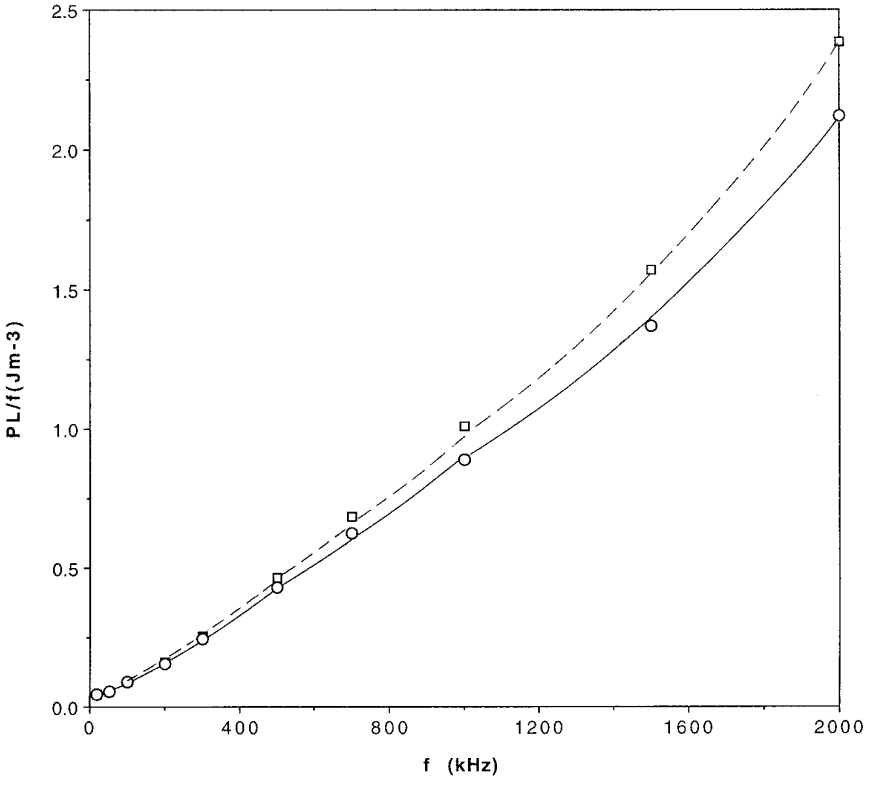

FIG. 10. Power losses at 50 mT and 323 K as a function of frequency. PL/*f* is plotted versus *f*. (□) sample A; (○) sample B.

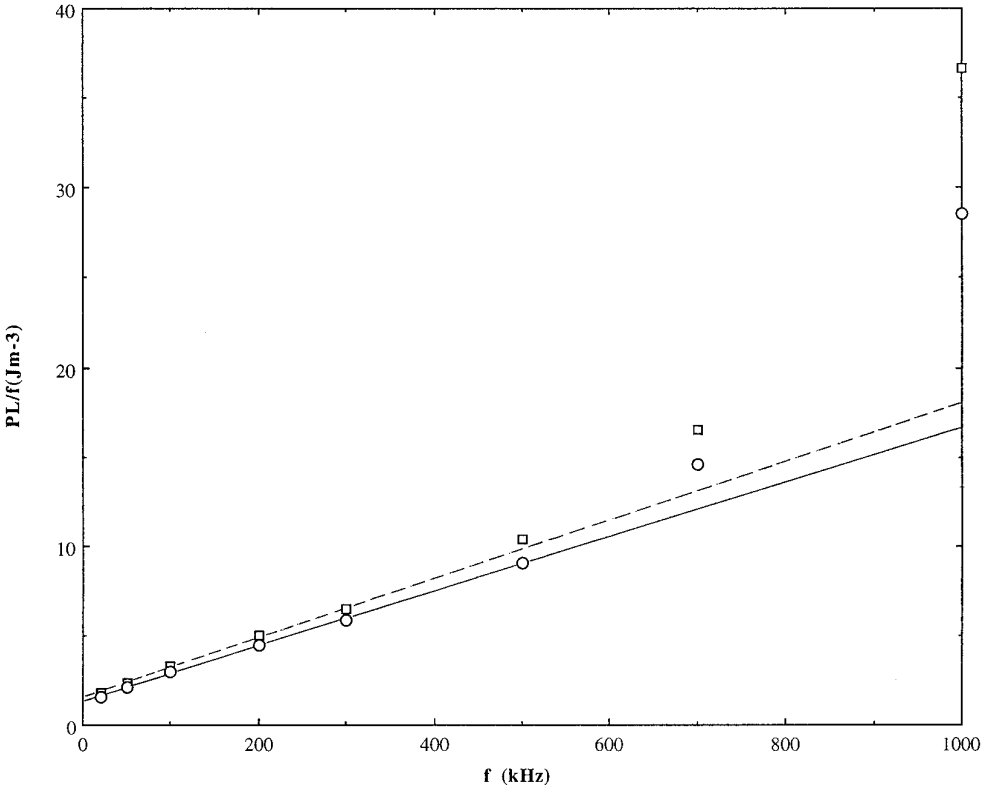

FIG. 11. Power losses at 200 mT and 323 K as a function of frequency. PL/*f* is plotted versus *f*. The solid and lines and broken lines represent the sum of the terms of hysteresis loss and eddy current loss for the undoped and doped sample, respectively. (□) sample A; (○) sample B.

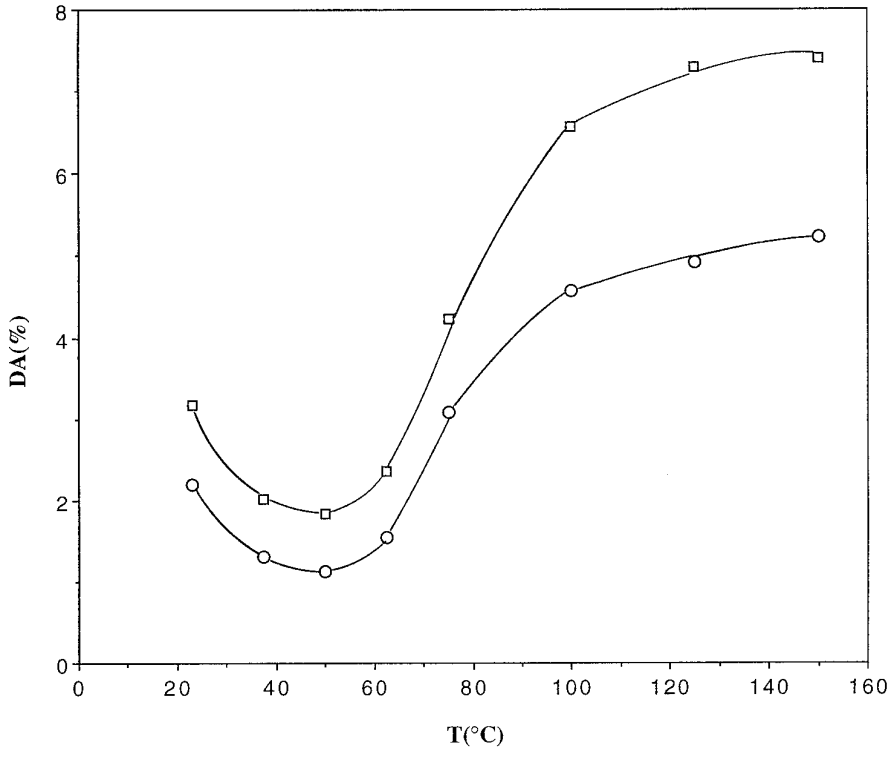

FIG. 12. Disaccommodation at 100 kHz as a function of temperature. (□) sample A; (○) sample B.

5. Required Property for The Third Additive other than CaO and SiO_2

As has been discussed, the essential character of Nb_2O_5 as a third additive other than CaO and SiO_2 for Mn–Zn ferrites may be expressed as the formation of the pairs of Nb^{5+}–Ca^{2+} and Nb^{5+}–Fe^{2+} in the grain boundary. If this character can be applied to other substances, the transition metal elements which have the valencies 4+ and 5+ would be the candidates. Indeed the additives of V_2O_5, Nb_2O_5, Ta_2O_5, TiO_2, ZrO_2, and HfO_2 have been shown to improve the magnetic properties (7). The combination of solubility of these additives in the spinel lattice, the melting point of the grain-boundary layer including these additives, and the sintering conditions would determine the microstructure and the magnetic property of Mn–Zn ferrites.

V. SUMMARY

The effect of Nb_2O_5 addition in Mn–Zn ferrites was investigated by observing the grain-boundary structure and measuring magnetic properties for the samples with additives of CaO–SiO_2 and CaO–SiO_2–Nb_2O_5.

(1) In the case of the sample without Nb_2O_5 addition, Ca and Si atoms concentrate near the grain boundary and are incorporated in the spinel lattice as far as 6 nm (half-width).

(2) In the case of the sample with Nb_2O_5 addition, Nb atoms concentrate in the grain boundary with a half-width of 2.5 nm and keep Ca atoms from being incorporated in the spinel lattice by pairing Nb^{5+} and Ca^{2+} ions.

(3) The addition of Nb_2O_5 slightly promotes the grain growth of Mn–Zn ferrites. This is thought to be due to lowering of the melting point of the (Fe, Mn, Zn)$_3O_4$–CaO–SiO_2–Nb_2O_5 system, which plays a major role in the liquid-phase sintering.

(4) Electrical conductivity of the sample with Nb_2O_5 addition is smaller with higher activation energy of 0.211 eV compared with the sample without Nb_2O_5 addition. This is thought to be due to the fact that Fe^{2+} ions are loosely bound with Nb^{5+} ions around grain boundaries.

(5) The addition of Nb_2O_5 makes initial permeability lower and hysteresis loss at 200 mT lower. The lower permeability is thought to be mainly due to the improper Fe^{2+} content in the bulk owing to the enrichment of Fe^{2+} ions around the grain boundary. The lower hysteresis loss is thought to be due to the decrease of internal stress of the lattice owing to pairing of Ca^{2+}–Nb^{5+} around the grain boundary.

(6) The term of residual loss becomes increasingly important above 500 kHz. The addition of Nb_2O_5 is thought

to reduce the term of resonance of the domain wall motion and/or spin rotation, since initial permeability of the sample with Nb_2O_5 addition is smaller and the resonance frequency is higher. The addition of Nb_2O_5 is thought to also reduce the term of diffusion magnetic aftereffect due to the migration of Fe^{2+} ions into cation vacancies under the magnetic field at high frequencies, since disaccommodation of the sample with Nb_2O_5 is about 30% less than that of the sample without Nb_2O_5.

REFERENCES

1. T. Akashi, *Trans. Jpn. Inst. Metals* **2,** 171 (1961).
2. P. E. C. Franken and W. T. Stacy, *J. Am. Ceram. Soc.* **63**(5–6), 315 (1980).
3. S. Otobe and T. Mochizuki, *in* ''Ferrites: Proceedings of The Sixth International Conference on Ferrites, Tokyo,'' ICF6, p. 329. 1992.
4. H. Tsunekawa, A. Nakata, T. Kamijo, K. Okutani, R. K. Mishra, and G. Thomas, *IEEE Trans. Mag.* **MAG-15**(6), 1855 (1979).
5. A. Znidarsic, M. Limpel, G. Drazic, and M. Drofenik, *in* ''Ferrites: Proceedings of The Sixth International Conference on Ferrites, Tokyo,'' ICF6, p. 333. 1992.
6. K. Ishino, S. Satoh, Y. Takahashi, K. Iwasaki, and N. Obata, *in* ''Ferrites: Proceedings of The Sixth International Conference on Ferrites, Tokyo,'' ICF6. 1992.
7. E. Otsuki, S. Yamada, T. Otsuka, K. Shoji, and T. Sato, *J. Appl. Phys.* **69**(6), 5942 (1991).
8. E. Otsuki, *Tokin Tech. Rev.* **19,** 24 (1993).
9. P. E. C. Franken and H. van Doveren, *Ber. Dt. Keram. Ges.* **55**(6), 287 (1978).
10. Japanese Industrial Standards, JIS M 8213-1983 (1983).
11. Japanese Industrial Standards, JIS M 8212-1983 (1983).
12. Japanese Industrial Standards, JIS M 8215-1983 (1983).
13. Japanese Industrial Standards, JIS M 8228-1983 (1983).
14. H. T. Kin and H. B. Im, *IEEE Trans. Mag.* **MAG-18**(6), 1541 (1982).
15. H. Yoshimatsu and T. Narutani, private communication.
16. T. Sato and Y. Sakaki, *Electron. Commun. Jpn. 2,* **72**(6), 42 (1989).
17. A. Braginski, *Phys. Status Solidi* **11,** 603 (1965).